AEA FUS 250

AEA Technology
Fusion
(Euratom/UKAEA Fusion Association)

Thermal-Structural Analysis and Modelling of First Wall Concepts

Panayiotis J Karditsas

27 September 1993

AEA Technology
Fusion

Culham
Abingdon, Oxfordshire
OX14 3DB
United Kingdom
(Euratom/UKAEA Association)
Telephone 0235–464277
Facsimile 0235–463435

ABSTRACT

The thermal–structural behaviour and performance of fusion power plant first wall concepts is analysed with the aid of a finite element analysis code and conclusions are drawn. This study is an integral part of a wider research effort undertaken by AEA Technology, which involves the development of methods for detailed assessment of fusion related systems and components. The performance of the first wall depends, under normal operating conditions, on the thermal loading conditions and internal coolant (if any) pressure loading conditions, and during a disruption also depends on the induced magnetic pressure (force). The thermal and structural analysis comprises performance comparisons of rectangular, circular and elliptical cross section cooling channels, assuming as first wall structural materials the austenitic (316) and martensitic (Manet) stainless steels and a Vanadium alloy. A parametric study is included with variable surface heat flux, in the range 0.1–0.6 MW/m^2 and volumetric heat flux in the range 15–25 MW/m^3. For steady state operation, the maximum temperature is in the range of 550–650 C, maximum thermal stress in the range of 150–650 MPa and maximum strain in the range of 0.13–0.27. In general the designs examined are shown to be capable of withstanding the loading conditions imposed, although the effect of such factors as pulsed or part load operation should be carefully examined.

1. INTRODUCTION

The first wall physically exists between the blanket and the plasma, and is either integrated to the blanket or exists as a separate entity. The major function of the first wall is the protection of the blanket from any violent plasma activity (like a disruption), the provision of the necessary ultra-clean plasma conditions needed in order to initiate and sustain the plasma and the protection against particles and radiation originating from the plasma.

The experience gained from presently operating large experimental tokamaks is valuable and provides a guide in order to correctly anticipate potential problems in the design of fusion power plants. Major design features of existing experimental tokamaks are the pulse mode of operation and the expected plasma disruptions, both critical problems for the successful design and expected lifetime of components.

Although the basic configuration of the tokamak in a power plant will be similar to existing machines, it is anticipated that the severity of plasma disruptions (a few major or many minor or a combination), possible pulsed operation and power loading fluctuations, will be critical issues for power tokamaks operating at higher fusion power loads and higher in-vessel component temperatures which are required for net electricity production. The choice of a final first wall design concept to be adopted for use in a power plant depends on a combination of thermal, structural and plasma driven operational regimes, limitations and constraints.

In studies and conceptual designs of DEMO fusion power plants [1–6], next step and experimental tokamaks [7–11] or other publicised work on this subject, for example [12–14], various proposals of first wall concepts and designs exist, with a large number appearing under blanket design concepts, which can collectively be described as:

(a) single plate, integral to the blanket pressure vessel and cooled either internally or by the blanket coolant,

(b) bare plate internally cooled, independent of the blanket cooling circuit, and either exposed to the blanket coolant or backed by the blanket material,

(c) plate externally or internally cooled, with protective tiles (or coating) cooled either by heat conduction or radiation to the plate.

This study presents the philosophy, the criteria and imposed constraints and limitations that are relevant to the thermal-structural design of the first wall of a fusion power plant and includes several examples. The focus is on concepts involving internally cooled first wall options, since the demonstrated span for a single plate/blanket vessel design based on loading conditions similar to a fusion power plant is deemed small (less than 20 cm), thus limiting the selection range. Also, the protection of the structure from global or local plasma events, a process requiring the dissipation of large amounts of energy (heat) and the sustainment of induced excessive thermal stresses, requires a cooling circuit independent of the blanket.

The thermal-structural analysis accounts for temperature dependent thermal and structural material properties, involves various cooling channel cross sections and includes a parametric exercise in thermal loading conditions.

2. DESIGN PHILOSOPHY

The design of a reliable first wall for a fusion power plant presents many engineering challenges and is dependent on the choice of such plant parameters as steady or pulsed operation, fusion power and electrical power output (power loading). It is also dependent on the availability of licensed nuclear materials and structural–thermal loading conditions during normal operation and during plasma disruptions which result in excursions of the thermal–structural conditions. In present day and future experimental tokamaks it is assumed and expected that plasma disruptions are a common feature and the designer has to make allowances for that. But in fusion power plant tokamaks it is anticipated that there will be only one major disruption with possibly a small number of minor disruptions during the lifetime of the machine, a requirement for licensing such power plants. Also, the first wall will either have a protective coating or tile, or provisions must be made for passive means to deter the plasma from touching the surface, although the occurrence of a highly localised plasma activity would be damaging to the wall.

The comparative lifetimes of blanket and first wall are among the decisive factors for the concept to be employed. A separate first wall concept will provide versatility and allow the independent replacement of first wall and blanket module, thus disengaging their service life. It will also provide for a separate cooling circuit in the vicinity of the blanket. Therefore, the frequency of disruptions will determine whether the first wall will be integrated to the blanket or a separate structure and the severity of disruptions will determine whether a protective coating (or tile) will be needed or the surface will be bare with provisions for passive protection of the surface.

2.1 Critical issues

The first wall function and the resulting constraints and limitations can be grouped to those related to plasma surface interactions and those related to structural integrity and safety issues. Plasma-surface interactions in the form of energetic particles falling on the surface (impinging and reflecting) result in sputtering and the subsequent erosion of the first wall material (or coating-tile). The rate of erosion is dependent on the number of particles, the target material binding energy and the energy of the incoming particles, which is dependent on edge plasma density and temperature. The plasma, depending on the operational mode, can accommodate a specific maximum amount of impurities of a specific maximum effective atomic number, Z_{eff}. This is a constraint imposed by the maximum radiative loss of energy that the plasma can tolerate and which is directly proportional to the number of impurity particles and their effective atomic number. An increase in either one of these parameters, beyond what can be tolerated, results in a plasma disruption and loss of power. This effect is critical during the start-up and heating phases (in a pulsed machine) of operation of the tokamak.

Low Z materials erode considerably but high Z materials are more resistant to erosion. Ideally, a medium or high Z material first wall could be tolerated during normal operation but a low Z coating will be required during the start-up and heating phases. In addition to considerations of low or high Z, high vapour pressure materials to be used as coatings or for the tiles, will evaporate more readily at the higher working temperatures of these components and this loss of material mechanism is in addition to the erosion due to sputtering. Also, high Z materials require increased cooling due to the high gamma photon absorption and the resulting increased heat loads.

The various loading conditions encountered during the operation of a tokamak result in structural effects such as thermal stresses from loads induced by neutron interactions with the structural material, plasma radiation and particle impingement, equivalent membrane and bending stresses induced by the coolant pressure and plasma decay induced electromagnetic forces following a disruption. As a result, the operating conditions and loads lead to structural damage and failure by such mechanisms as yielding, thermal creep rupture and fatigue due to thermal cycling, plastic strain cycling (ratcheting), crack growth–propagation and radiation induced swelling and creep. In general, the effect of neutron damage inflicted onto the structural materials and the degradation of key properties is of major concern in the design and lifetime prediction of first wall structures. Taking into consideration all the possible structure failure mechanisms, for a steady state tokamak the most likely are erosion and evaporation of the first wall material, yielding (excessive stress or crack initiation–growth) and thermal creep rupture, whereas for a pulsed tokamak combinations of fatigue–creep or creep–plasticity mechanisms and crack initiation–growth induced under cyclic fluctuating and variable loads.

In general, materials with high thermal conductivity, heat capacity and yield strength and low modulus of elasticity, thermal expansion coefficient and activation are desirable for the construction of the first wall because they resist thermal transients and thermal fatigue, generate minimum amount of waste and retain their structural integrity at the high operating temperatures and under the incoming neutron flux. Thermal fatigue will in general rule out first wall concepts based on thick melting-ablative layers (due to crack growth-propagation) and thermal cycling, which is the driving force for thermal fatigue, will be present unless the operation of the tokamak is steady.

2.2 Thermal - Structural Loading

Thermal loading of the first wall comprises steady and transient sources of energy and structural loads with induced stresses, as follows:

1. The *volumetric heat deposition* q_n in W/m^3, is a result of the interaction between the structural material and the incoming neutrons and secondary photons. This load is material and blanket design dependent and is calculated by a proper neutronic analysis of the first wall, blanket and shield. The heat deposition assumes peak values on the torus midplane at the inboard and outboard blankets and calculations show that there is a poloidal variation with values as low as $q_n/4$ at the top and bottom of the torus [15–16]. Reference [12] gives typical heat deposition values of 10 MW/m^3 in 316 stainless steel, 11 MW/m^3 in molybdenum, 7 MW/m^3 in silicon carbide, for 1 MW/m^2 wall loading which is equivalent to a neutron flux of 4.48×10^{17} n/m^2–s of 14 MeV energy neutrons. Typical peak values for fusion power plants and experimental machines, depending on design and configuration, are in the range of 10–40 MW/m^3. This heat source is either continuous for steady state operation or ranges between 30–300 s for power plant tokamaks with pulsed operation [17] or ranges between 100–2000 s in experimental and next step machines.

2. The *surface heat deposition* q_s in W/m^2, is a result of energetic particle impingement on the surface, plasma radiation (from impurities and Bremsstrahlung) and particle transport. Typical peak values for experimental machines and fusion power plants, depending on plasma conditions (density, temperature, impurity level), are in the range of 0.1–0.6 MW/m^2.

3. The *transient thermal load* is a result of a plasma disruption, when the plasma thermal energy is deposited on the first wall in a small period of time. Ideally the power will be deposited uniformly over the entire surface but some concentration due to runaway electrons will be unavoidable. Typical energy–time values are in the range of 400–1000 MJ and 10–100 ms for a fusion power plant and 0.1–5 ms in next step and experimental machines [1,7,10,12]. The plasma thermal energy in J, is given by:

$$Q_{dis} = \left(\tfrac{3}{2} n k_o T\right) V_{plasma} \tag{1}$$

$$V_{plasma} = 2\pi^2 R a_p \kappa \tag{2}$$

with n the plasma density in m^{-3}, k_o=1.38x10^{-23} J/K the Boltzmann constant, T the plasma temperature in K, R the major and a_p the minor plasma radii in m and κ the plasma elongation. The equivalent heat flux in W/m^2 corresponding to the disruption energy and deposited on a flat surface A_{fw} in m^2, can be calculated from:

$$q_{dis} = \frac{Q_{dis}}{A_{fw}\,\tau_{dis}} \tag{3}$$

$$A_{fw} = 4\pi^2 R a_p \sqrt{\tfrac{1}{2}\left(1+\kappa^2\right)}\, f_a \tag{4}$$

with τ_{dis} the disruption time constant and f_a the ratio of first wall surface to plasma surface. Typically, f_a is ranging between 1.1 and 1.15 and κ between 1.5 to 3.

4. The *steady primary stresses* induced as a result of the coolant pressure p in Pa. The type of coolant, maximum thermal loading conditions, pumping power restrictions and cooling channel geometry determine the coolant pressure needed. Typical values of the pressure for helium and water, the prime coolant candidates for fusion power plants, range between 2–20 MPa with pressurised water being at the high end of the range.

5. The *steady secondary stresses* induced as a result of the temperature gradients in the material, dependent on the temperature gradient in the material.

6. The *electromagnetic force or pressure* induced by the action of the toroidal component of the plasma current decay with the poloidal magnetic field (JxB effect). During normal operation the electromagnetic forces are negligible, but during a disruption typical values of magnetic pressure are in the range of 1–3 MPa. This load is superimposed on the other structural loads during steady operation.

It should be pointed out that during a major disruption which is followed by plasma loss, the heat loads will diminish and the only significant thermal load present will be the transient thermal deposition of the plasma energy on the surface.

3. THERMAL-HYDRAULIC ANALYSIS

The important parameters for an independently cooled first wall concept are the heat transfer coefficient, pressure drop and pumping power. The objective of the design is to maximise heat removal, minimise the pumping power to achieve it and ensure that the maximum temperature in the structure is as close as possible to the coolant temperature. These parameters depend on mass flow rate, cooling channel geometry, type of coolant used and coolant properties. Fig. 1 shows typical geometry with dimensions of independently cooled first wall designs.

The total power deposition on the first wall P_{fw} in W comprises the volumetric q_n and flat surface(=wL) q_{so} heat transfer terms, to be removed by N_c cooling channels, calculated from:

$$N_c = \frac{A_{fw}}{wL} \tag{5}$$

with w in meters the cooling channel pitch and L in meters the length of the first wall. An energy balance in one segment of the first wall, of width w and height H, under steady state conditions gives:

$$P_1 = \begin{cases} \dot{m} c_p \Delta T_c = q_n V_1 + q_{so} A_1 = h(SL)\Delta T_{cs} & \text{(a)} \\ P_{fw} \dfrac{wL}{A_{fw}} & \text{(b)} \end{cases} \tag{6}$$

with P_1 the single channel power in W, V_1 in m^3 and A_1 in m^2 the volume and surface area respectively, c_p the coolant specific heat capacity in J/kg–K, ΔT_c the coolant outlet to inlet temperature difference in K, $\dot{m}$ the coolant mass flow rate in kg/s, h the heat transfer coefficient in W/m^2–K and ΔT_{cs} the surface to coolant temperature difference in K. The volume and surface area for the first wall configurations as in Fig. 1, can in general be expressed as:

$$A_1 = f_1 wL \tag{7}$$

$$V_1 = f_2 wLH \tag{8}$$

with f_1 and f_2 the respective fractions which are dependent on the exact first wall geometry and S in meters the cooling channel perimeter. Table I lists all the relevant geometry and thermal-hydraulics parameters for rectangular, circular and elliptical cross sectional area cooling channels. Using equations 7–8 into equation 6(a), an expression for the mass flow rate is derived, as follows:

$$\dot{m} = \left(f_1 q_{so} + f_2 H q_n\right) \frac{wL}{c_p \Delta T_c} \tag{9}$$

The heat transfer coefficient h, friction factor f (Moody as opposed to Fanning $f'=f/4$) and pressure drop Δp in Pa, are dependent on the mass flow rate, the channel hydraulic diameter D_h in meters, channel perimeter S and the prevailing flow conditions (laminar, turbulent flow). Expressions are derived from appropriate correlations [18–19], as follows:

$$h = a_1 \left(\frac{4\dot{m}}{\mu S}\right)^{b_1} Pr^{c_1} \frac{k}{D_h} = C_1(T) \left(\frac{\dot{m}}{S}\right)^{b_1} D_h^{-1} \tag{10}$$

$$f = a_2 \left(\frac{4\dot{m}}{\mu S}\right)^{b_2} = C_2(T) \left(\frac{\dot{m}}{S}\right)^{b_2} \tag{11}$$

$$\Delta p = f \frac{L}{D_h} \left(\frac{1}{2} \rho U^2\right) = C_3(T) \left(\frac{\dot{m}}{S}\right)^{(2+b_2)} \left(\frac{L}{D_h^3}\right) \rho^{-1} \tag{12}$$

with, the constants a_1, a_2, b_1, b_2 and c_1 depending on the flow conditions, S and D_h on the channel shape, μ the viscosity in Ns/m^2, ρ the density in kg/m^3 and Pr the Prandtl number, all dependent on the coolant type. The pumping power, P_{p1} in W, for a single channel and total, P_{pump} in W, are given by:

$$P_{p1} = \dot{m}\frac{\Delta p}{\rho} = C_3(T)\left(\frac{L}{D_h^3}\right)\left(\frac{\dot{m}^{(3+b_2)}}{S^{(2+b_2)}}\right)\rho^{-2} \tag{13}$$

$$P_{pump} = C_3(T)\left(\frac{A_{fw}}{wD_h^3}\right)\left(\frac{\dot{m}^{(3+b_2)}}{S^{(2+b_2)}}\right)\rho^{-2} \tag{14}$$

with the temperature and coolant dependent constants defined by the following:

$$C_1 = a_1 k \mathrm{Pr}^{c_1}\left(4/\mu\right)^{b_1} \quad C_2 = a_2\left(4/\mu\right)^{b_2} \quad C_3 = 8C_2 \tag{15}$$

Using the Ditus–Boelter and Blasius correlations [18–19] for the heat transfer coefficient and friction factor, the constants are a_1=0.023, a_2=[0.316 (Re<10^5), 0.184 (Re>10^5)], b_1=0.8, b_2=[–0.25 (Re<10^5), –0.20 (Re>10^5)], c_1=[0.4 (heating), 0.3 (cooling)] for turbulent flow and a_1=4.364, a_2=64 (circular channel only, for other shapes different [19]), b_1=0, b_2=–1, c_1=0 for laminar flow.

The maximum temperature that occurs in the solid can be kept within acceptable limits, provided the heat load is transferred efficiently to the coolant. This implies large material thermal conductivity and small temperature gradients in the solid itself but also across the interface with the coolant. An expression for the latter, involving the primary parameters, is derived using equations 6(a) and 10 as follows:

$$\Delta T_{cs} = \frac{D_h}{S^{1-b_1}}\left(\frac{w}{\dot{m}^{b_1}}\right)\left(f_1 q_{so} + f_2 H q_n\right)\frac{1}{C_1} \tag{16}$$

The coolant pressure or density do not directly affect the heat transfer capacity of the coolant but do affect the pumping power. A high coolant density or pressure is important if the pumping power is to be kept low. In principle, a similar effect can be achieved by the employment of larger size (S and D_h) cooling channels but at the expense of heat removal capability, since the convected heat transfer rate decreases with increasing hydraulic diameter. Although the single channel pumping power is dependent on the channel length the total pumping power is not, but both are inversely proportional to the channel width w. Provided the mass flow rate stays the same, P_{p1} can be minimised if w and D_h are large, but this should be weighted against smaller h and larger T_{max} in the solid. The choice of dimensions and shape of the cooling channels must be weighted such that h, T_{max} and P_{p1} are within acceptable limits. Optimization of these parameters is beyond the scope of this study, but can be easily implemented using equations 5–16.

4. STRUCTURAL ANALYSIS

The structural integrity of the fusion power plant first wall must be maintained throughout the lifetime of the component. The criteria by which the design is assessed must be identified and tailored to the particular application. First wall structures are classified by, and will be restricted by the design codes relevant to medium and high temperature power plant environments. Typical

examples are the ASME Boiler and Pressure Vessels Code, the BS 5500 and the ASME Code Case N–47 particular to high temperature operation of components of heat resistant alloys, possibly subjected to cyclic loading [20–22]. The codes distinguish between failure criteria under steady load and under cyclic load and lay down rules for failure prediction under combined creep–plasticity and creep–fatigue conditions. First wall problems particular to fusion are thermal stresses and the structural damage due to irradiation.

Thermal stress – In the codes, stresses are categorized into primary caused by the mechanical loads and secondary caused internally in the structure. Thermal stresses belong to the latter category and are generated either by external constraints and loads that prevent the structure from free movement or internally from the temperature differential across various parts of the solid which causes variations in the natural expansion [23]. In general the temperature distribution in the solid induces thermal stresses and possibly bending moments [24]. The stress is given by:

$$\sigma_{th} \propto \alpha E\left(\hat{T} - T\right) \tag{17}$$

with α the coefficient of thermal expansion in m/m-K, E the modulus of elasticity in N/m^2, T the material temperature in K and $\hat{T}$ the average material temperature (or temperature at zero thermal stress). A negative σ_{th} means compression whereas a positive tension, which implies that the colder parts of the structure with $T<\hat{T}$ will be under tension whereas the hotter parts with $T>\hat{T}$ will be under compression. The effect of a steep temperature gradient is to induce large thermal stresses and care should be taken in the design to avoid such gradients during thermal shock conditions.

Fig. 2 shows a typical power duty cycle where the structure is subjected to cyclic thermal stressing as the temperature changes between T_d and T_c. The parts of the structure at or around T_{max} are experiencing the largest stress and most likely will be in the plastic or creep range, whereas the parts at or around T_{min} will still be at the elastic range. This is of interest in the application of the codes, where elastic design analysis restrictions are relaxed without requiring a full inelastic analysis, in the belief that very localised stresses will not lead to ratcheting and that the surrounding material will restrain any low cycle fatigue in these areas.

Irradiation damage–creep – neutron fluxes can lead to structural damage through the mechanisms of void swelling and creep [25] and changes to material properties [26]. Both mechanisms must be accounted in the calculation of primary and secondary stresses used in design codes. Swelling, which is caused by vacancies combining into voids, varies linearly with dpa after a certain threshold has been exceeded. Irradiation creep ε_{irr} can be expressed as:

$$\varepsilon_{irr} = c\,\Phi\,\frac{\sigma}{E}\,t_c \tag{18}$$

with c a constant, Φ the neutron flux in n/m^2–s, σ the stress due to mechanical loading and t_c the time to reach the strain ε_{irr}. For pulsed operation and during dwell times, irradiation creep causes stress relaxation during the "on" period and stress reversal during the "off" period, which could lead to considerable reduction in component lifetime or brittle fracture during maintenance unless the material has a low ductile to brittle transition temperature.

Failure prediction and lifetime – The primary and secondary stresses are used in the codes to define the allowable or admissible stress limits in order to avoid failure and predict the component lifetime under the actual imposed loading conditions [20–22,25,27].

For steady loading conditions design against failure defines allowable stress (σ_a) limits, as given by comparison of the stationary (S_m) to the time dependent ($S_{m,t}$) stress state of the material, as follows [20,25,27]:

1. For primary membrane stress load $\sigma_a = S_{m,t}$
2. For primary membrane + bending stress loads $\sigma_a = 1.5\, S_{m,t}$
3. For primary + bending + secondary stress loads $\sigma_a = 3\, S_m$

$$S_m = \min\left[\tfrac{2}{3}\sigma_y, \tfrac{1}{3}\sigma_u\right] \quad \text{and} \quad S_{m,t} = \min\left[S_m, \tfrac{2}{3}\sigma_{r,t}, \tfrac{1}{3}\sigma_{0.1,t}\right] \tag{19}$$

with σ_y the 0.2% yield strength, σ_u the ultimate tensile strength, $\sigma_{r,t}$ the stress for creep rupture in time t and $\sigma_{0.1,t}$ the stress to produce 0.1% strain in time t. It should be pointed out that a brittle material will resist failure more if it is subjected to compressive rather than tensile loads. Service life can be estimated by the creep rupture stress–lifetime curves at the maximum stress point in the structure.

Cyclic loading conditions are dealt with by the design codes depending on the working range and combination of loading conditions. The allowable stress method can be applied in the creep range, assuming that the structure will yield during the first few cycles and internal residual stresses will inhibit any further yielding and the structure will "shakedown" to elastic behaviour [27,28]. This can be dealt with by relaxation of the restrictions of the elastic route of the code without an inelastic analysis. The modified limits for "shakedown" are [25,27] as follows:

1. For primary membrane stress load $\sigma_a = 0.6\,[n/(n+1)]\,\sigma_y$
2. For primary membrane + bending stress loads $\sigma_a = 0.9\,[n/(n+1)]\,\sigma_y$
3. For primary + bending + secondary stress loads $\sigma_a = 1.8\,[n/(n+1)]\,\sigma_y$

with n the creep law exponent, determined from the slope of the isochronous creep strain against log stress curve. For metals n ranges between 3 and 7, with $n \to \infty$ denoting rigid–plastic behaviour.

The design codes [20,22] use the Bree diagram, a schematic shown Fig. 3, as a first assessment tool for determining the working range and whether cyclic plasticity or ratcheting (cyclic plastic strain) conditions prevail. The location of the boundaries in the diagram will change if the Bree assumptions of elastic–perfect plastic material and linear temperature variation are violated. The thermal cyclic stress is defined as $\Delta\sigma_{th}=\alpha E\Delta T/2$ and σ_m is the mechanical loading. In general cyclic plasticity and ratcheting are assumed to always lead to failure and must be avoided in the design.

The prediction of lifetime of the component is of interest and important as a design criterion. At steady loading conditions it can be obtained from the creep rupture stress or strain versus lifetime curves for the material, for example the Larson–Miller parameter [27,28]. Under variable or cyclic load conditions the lifetime can be obtained as follows:

1. For a crack–free material, the fatigue usage factor (Miner's rule) is defined as:

$$U_f = \sum_i N_i / N_{fi} \le w \tag{20}$$

with N_i the number of cycles of type "i" strain range and N_{fi} the number of cycles to fatigue failure at this strain range. If the stain range is the same for every cycle or load variation then

N_i becomes N_{fi} and the lifetime is obtained from the $\Delta\varepsilon$–N_f curve for the material. The value of w is usually taken as w=1.0.

2. For a material with initial cracks the lifetime is obtained from the da/dN (a=crack size, N number of cycles) against stress intensity factor ΔK relationship [25,27,28].

3. In general cyclic stress will fatigue the material while creep damage will occur during periods of steady operation (irradiation, high thermal stresses). In order to implement both effects the design codes [20,27] assume a combined damage summation rule must be satisfied with:

$$U_f + U_c = \sum_i {N_i}/{N_{fi}} + \sum_i {t_i}/{t_{ri}} \le w \tag{21}$$

with t_i the load "i" duration and t_{ri} the time to creep rupture at a given load level "i" and N_i, N_{fi} as defined before, w taken as w=1.0. An overall equivalent lifetime t_o can be estimated from the fatigue life t_f and the creep life t_c defined as follows:

$$t_o = \left({1}/{t_f} + {1}/{t_c} \right)^{-1} \tag{22}$$

For example, calculations of the stress–strain resulting from the thermal and mechanical loads, allows the estimation of the number of cycles (and t_f) for fatigue failure from the strain–lifetime curves and of the creep rupture time t_c using the primary or thermal stress in the appropriate creep law (thermal and/or irradiation creep). The number of cycles for fatigue for a first wall duty cycle as depicted in Fig. 3, gives:

$$t_f = N_f \left(t_{burn} + t_{dwell} \right) \tag{23}$$

Component lifetime due to erosion and evaporation, under steady or variable load conditions, can be estimated from the available respective rates $\dot{r}$ in m/yr and given by t~s/$\dot{r}$, with s in m the sacrificial layer of the bare wall or of the coating–tile. Typical values under various conditions can be found in [1,12,29–30]. Swelling due to neutron irradiation depends on dpa and lifetime estimation can be performed from available swelling–dpa–temperature correlations, for example [25]. Typically values in the range of 3–5% volumetric swelling are acceptable for the material [26].

A measure of the ability of materials to sustain the thermal stresses and resist fatigue failure are the thermal stress parameter M and the fatigue fracture quality factor defined as:

$$M = \frac{\alpha E}{(1-\nu)k} \qquad F = \frac{k \sigma_y}{\alpha E} \tag{24}$$

Materials with low M and high F are advantageous in the design of the first wall.

5. RESULTS AND FINITE ELEMENT ANALYSIS

The finite element code COSMOS/M [31] is used for performing thermal and structural analysis of the first wall. The thermal analysis module requires as boundary condition input, values of the local heat transfer coefficient h and coolant temperature T_c. The linear structural analysis module requires the temperature distribution in the solid, from the thermal analysis, for the calculation of the thermal stresses, the coolant pressure for the calculation of the primary stresses

and boundary conditions. This study considers plane two dimensional elements, with x–direction being radial, y–direction poloidal and z–direction toroidal, with generalised plane strain conditions, restrained boundaries and restricted bending in the z or toroidal direction.

The thermal–hydraulics and structural analysis results are displayed in Figs. 4–13, with the *equivalent flat surface* heat flux q_{so} in the range 0.1–0.6 MW/m^2 and the volumetric heat flux q_n in the range 15–25 MW/m^3 (for stainless steel ~1.5–2.5 MW/m^2 wall loading), for the three channel shapes as in Fig. 1, and three types of materials. The coolant is assumed to be helium at 5 MPa and 300 C and the coolant temperature rise is taken as ΔT_c=80 K, assuming an inlet of 260 C and an exit of 340 C.

The specification of tokamak and overall first wall dimensions and heat loads, allows for the calculation of mass flow rate, heat transfer coefficient, pumping power loss and total first wall power. The calculations in this study assume: major plasma radius R=7.5 m, minor a_p=2 m, elongation κ=1.6, area factor f_a=1.1, width w=30 mm (20 mm for circular channel), height H=25 mm, diameter D=10 mm (circular channel), major length a=20 mm, minor length b=10 mm (rectangular channel), major radius a=10 mm, minor radius b=5 mm (elliptical channel), support plate thickness s_1=10 mm, plasma facing plate thickness s_2=5 mm and channel length L=1000 mm. The load factors f_1 and f_2 are calculated using the expressions in Table I.

The loading conditions result in the mass flow rate being highest in the rectangular channel followed by the elliptical and circular channels, Fig. 4. Also, the overall dimensions used for the three channels yield the lowest D_h and S values for the circular channel (10 mm, 31.416 mm), whereas for the others are: rectangular (13.33 mm, 60 mm) and elliptical (12.96mm, 48.47 mm). The mass flow rate diminishes with q_n for the same q_{so}, Fig. 5.

The low $\dot{m}$ values for the circular channel do not result in the lowest h values, because the D_h and S values counterbalance that. A comparison of elliptical and rectangular channel h values, Fig. 6, shows that the lower D_h and S values of the elliptical channel result in higher h values despite the lower $\dot{m}$ in the elliptical channel. Therefore, in order to achieve maximum h values, it is more effective to decrease the dimensions of the cooling channel rather than increase the mass flow rate. The actions to increase h values, either by smaller dimensions or larger mass flow, result in an increase of pumping power, Fig. 8.

The two dimensional temperature and Von Mises thermal stress distributions for the rectangular, circular and elliptic channels, for a MANET first wall, are shown in Fig. 10, with q_n=25 MW/m^3, q_{so}=0.5 MW/m^2. The heat transfer coefficients are 4877.8, 6770.7 and 5246.3 W/m^2–K and the maximum primary stresses are 37, 13 and 36 MPa, for the rectangular, circular and elliptical channels respectively.

Thermal and structural finite element analysis for the rectangular channel, is performed with q_{so} in the range 0.1–0.6 MW/m^2, q_n=25 MW/m^3 and h in the range 3166.1–5280.9 W/m^2–K, assuming the austenitic 316 SS as first wall material. The calculations are repeated for MANET (martensitic stainless steel) and vanadium alloy V–15Cr–5Ti. The maximum temperature and % engineering strain variation with q_{so} are shown in Figs. 11–12, and the maximum thermal stress, σ_{max} and the stress at maximum temperature, σ_{Tmax}, are shown in Fig. 13. In the working range of temperatures, the thermal conductivity of V–alloy is larger than in MANET, which is larger than in 316 SS and with the same material order, the modulus of elasticity and thermal expansion coefficient are lower. This combination of material properties results in lower maximum temperatures, temperature gradients, stresses and strains in the respective materials. The thermal stress parameter M and

fatigue factor F, at a temperature of 400 C, are 0.062, 12600 (V–alloy), 0.125, 5710 (MANET) and 0.211, 777 (316 SS) respectively and the requirement of low M, high F is most favourable for the V–alloy.

The results suggest that failure under steady load is most likely to occur at the maximum stress location which is observed at the point of minimum temperature. An equally bad or worse combination for failure can occur at the maximum temperature region provided the stresses in that region of the material exceed the allowable values. The structural analysis performed shows that for low values of q_{so} ($\leq$0.1 MW/m^2) the maximum thermal stress value is observed at the maximum temperature, a condition which is reversed (i.e. maximum stress at minimum temperature) when the effect of excessive heating on the plasma facing side of the first wall is dominant. This suggests that for a particular set of parameters (dimensions+flow+heat loading) there will be a minimum stress condition, a good design point. A variation in q_n and calculation of the maximum temperatures and stresses suggests that at the low q_{so} values the higher q_n results in larger temperatures and stresses, a condition reversed at higher q_{so}. Therefore, the combined effect of high q_{so} with low q_n results in worse conditions as compared to both being high. These observations suggest that a balance point can be observed if there is some heating allowed from the blanket side, although this has to be investigated further. For the rectangular channel with q_n=25 MW/m^3, q_{so}=0.5 MW/m^2, the effect of:

1. Increasing the coolant pressure from 5 MPa to 10 MPa results in a maximum primary stress value of 74 MPa as opposed to 37 MPa. This result imposes a constraint on coolant pressure and it will be critical in a pressurised water system. For example the allowable stress for primary loads, for 316 SS operating at 500 C is ~110 MPa.

2. Decreasing ΔT_c from 80 K to 40 K results in an increase of mass flow by a factor of 2, h by a factor of 1.74 and pumping power by a factor of 6.94. The resulting maximum temperature and thermal stress become 517 C and 360 MPa from 564 C and 391 MPa respectively. This result indicates that the effect of increasing $\dot{m}$ and h values on the first wall temperature and thermal stress is minimal, but results in an order of magnitude increase of pumping power.

The prediction of failure and estimation of lifetime of the proposed designs is an ongoing process and beyond the scope of this study. As an example consider the case of 316 SS rectangular channel. The maximum allowable stress under steady operation is 80 MPa (primary) and 200 MPa (614 C), 240 MPa (357 C) (secondary). Since the secondary stress conditions are prevailing, the first wall will operate safely under a maximum of 0.15 MW/m^2 surface heat load with 25 MW/m^3 volumetric heat load, see Fig. 13. Assuming a cyclic operation at the previously stated heat load, with a variation in temperature between 300 C and 484 C, the induced cyclic stress variation is $\Delta\sigma_{th}$ ~265 MPa. The yield stress at 484 C is σ_y=113 MPa, and the Bree diagram for 316 SS at p_m=0.46 and σ_θ=2.35, indicates plasticity will occur at the high temperature region, but at the minimum temperature of ~375 C the yield stress is 122 MPa and the cyclic stress variation is $\Delta\sigma_{th}$~108 MPa and σ_θ=0.88, which indicates the material in that region is in the "shakedown" region. Therefore, under the cyclic operating conditions the structure will most probably fail.

For the vanadium alloy with steady operation at 25 MW/m^3 and 0.5 MW/m^2, the maximum allowable stress is 105 MPa (542 C), 125 MPa (360 C) (primary) and 315, 375 MPa respectively (secondary). At the above stated heat loading condition the secondary stress is, maximum 205 MPa

(at 360 C) and at maximum temperature (542 C) is 158 MPa, with the primary being 36 MPa. The structure will not fail under these conditions. If the operation is cyclic, with a variation between 300 C and 542 C, the induced cyclic stress variation is $\Delta\sigma_{th}$ ~145 MPa. The yield stress at 542 C is σ_y=200 MPa, and the Bree diagram at p_m=0.18 and σ_θ=0.725, indicates that the structure is entirely in the elastic region, therefore will not fail, but has very limited safety margins.

6. CONCLUSIONS

The first wall thermal and structural design philosophy and analysis tools have been presented and examined. The thermal analysis requires consistent data for the geometry, thermal loading conditions and coolant type–conditions. These data allow calculation of the temperature distribution in the structure with the aid of finite element codes. The thermal analysis results are in turn used in a structural analysis, which in this study is steady state and linear, but could also be non-linear and/or transient, to determine the stress and strain distributions. The stress and strain results are then used to predict failure and lifetime according to the rules laid down by the appropriate design codes. In particular the design is limited by and must resist failure due to:

1. Excessive primary and secondary stresses causing plasticity, crack initiation and growth, leading to yielding and creep rupture, a process characteristic of high temperature operation and enhanced by irradiation in the tokamak environment,

2. Erosion due to sputtering and evaporation, and

3. Fatigue due to excessive cyclic thermal stresses, strains, plasticity and fracture due to crack growth and propagation, all associated with pulsed operation and variations of the power output.

The results of the thermal and structural analysis calculations, lead to certain observations and conclusions that can be summarized as follows:

1. The design and choices are to a significant extent dependent on whether the operation is steady or pulsed,

2. The combined creep and fatigue observed in systems operating under a neutron flux is more severe than if the two mechanisms were acting independently. Creep in such systems is not only temperature dependent but also irradiation dependent and will therefore be present even at low operating temperatures,

3. The structure must be checked both at the point of maximum stress, which for the cases examined in this study occurs at the minimum temperature, and at the point of maximum temperature because the temperature-stress loading combination at that point could be worse than the loading at the maximum stress point,

4. In order to improve the heat transfer coefficient, it is more effective to decrease the channel dimensions rather than increase the mass flow rate,

5. When the value of the heat transfer coefficient is doubled, the maximum stress and temperature observed in the structure do not change proportionally, but the pumping power increases by an order of magnitude,

6. The induced temperature gradients in the structure are important. The combination of "large" surface heat fluxes with "low" volumetric heat fluxes creates unfavourable conditions and generates large temperature gradients. The calculations suggest that for given volumetric heat flux load and varying surface heat flux, there is an optimum temperature gradient (and thermal stress) point as the surface flux goes from "low" to "high" values. Therefore heating the structure on the blanket side is advantageous when these conditions prevail.

In general the design must lead to the lowest possible/allowable operating temperatures, small temperature gradients across the material and, for pulsed or load variation operation, must ensure the mean and/or maximum temperature is as close to the coolant temperature as possible in order to avoid excessive cyclic stresses. The various parameters for thermal and structural performance must be weighed against each other and optimisation of the shape and dimensions should be performed.

7. ACKNOWLEDGEMENT

This work was supported by AEA Technology internal research funds and by EURATOM. The author would like to thank Ian Cook, Neill Taylor and Christophe Sublet of the Strategic Studies Group, for their valuable comments and support in completing this study.

TABLE I

Geometry factors and thermal-hydraulic data

The parameters appearing in the expressions refer to the first wall geometry as presented in Fig. 1, with w the width, H the height, D the diameter, a the major axis or side, b the minor axis or side, s_1 the support plate thickness and s_2 the plasma facing side plate thickness.

	Rectangular	Circular	Elliptical
f_1^{-1}	1	$\frac{\pi}{2}$	$\frac{\pi}{4}\left[1.5\left(1+\frac{2(b+s_2)}{w}\right)-\sqrt{\frac{2(b+s_2)}{w}}\right]$
f_2	$1-\left(\frac{a}{w}\right)\left(\frac{b}{H}\right)$	$1-\frac{1}{2}\left(\frac{w}{H}\right)\left(1-\frac{\pi}{4}\right)-\frac{\pi}{4}\left(\frac{D^2}{wH}\right)$	$1-\left(1-\frac{\pi}{4}\right)\left(\frac{b+s_2}{H}\right)-\pi\left(\frac{a}{w}\right)\left(\frac{b}{H}\right)$
S	$2a\left(1+\frac{b}{a}\right)$	πD	$\pi a\left[1.5\left(1+\frac{b}{a}\right)-\sqrt{\frac{b}{a}}\right]$
D_h	$\frac{2b}{1+\frac{b}{a}}$	D	$\frac{4b}{1.5\left(1+\frac{b}{a}\right)-\sqrt{\frac{b}{a}}}$
A_c	ab	$\pi D^2/4$	πab

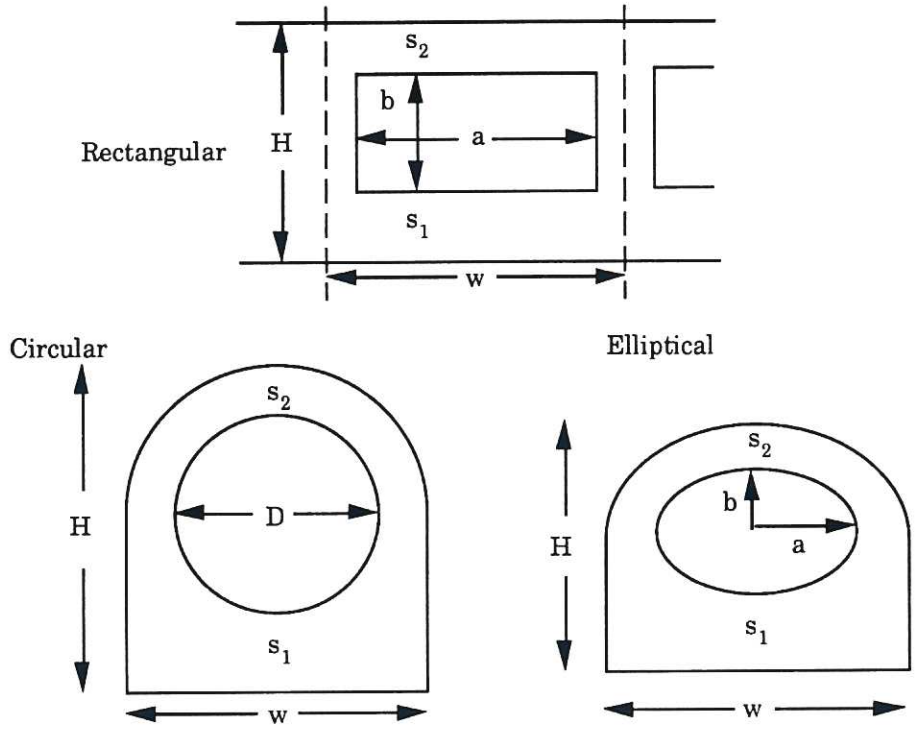

Figure 1: Typical first wall designs with variable cross sectional area cooling channels

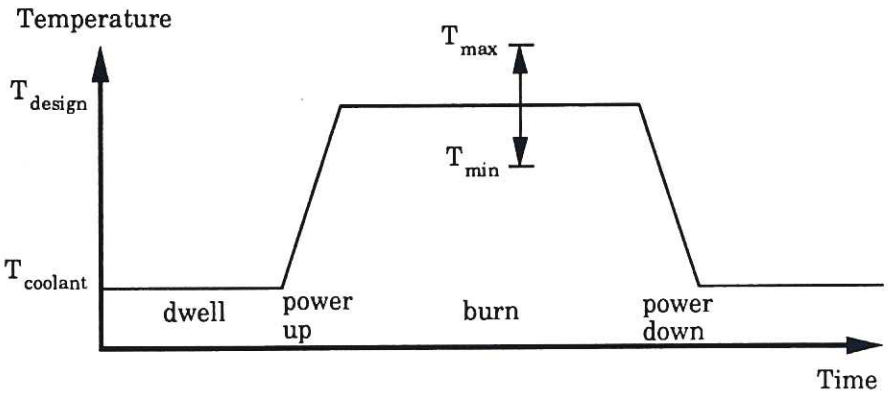

Figure 2: A typical fusion power plant duty cycle

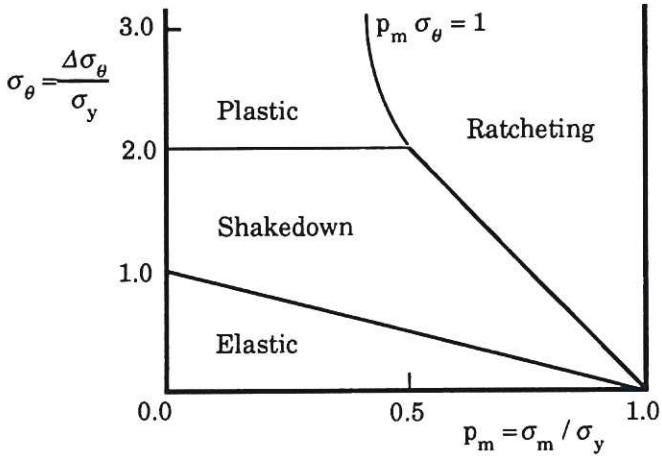

Figure 3: Bree diagram for combined creep–plasticity assessments.

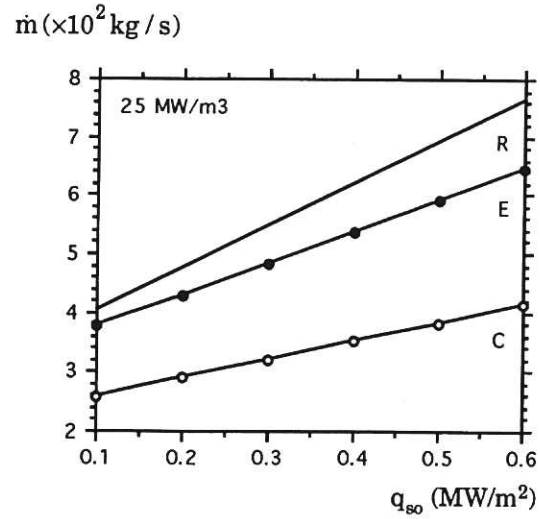

Fig. 4: The ṁ variation with q_{so} for the circular, rectangular and elliptical channels.

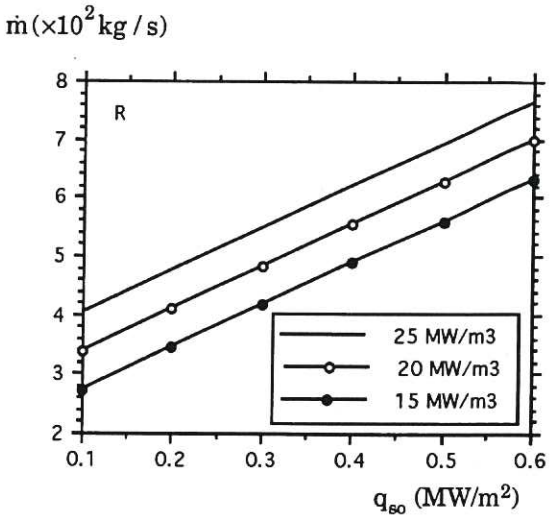

Fig. 5: The ṁ variation with q_{so} and q_n for the rectangular channel.

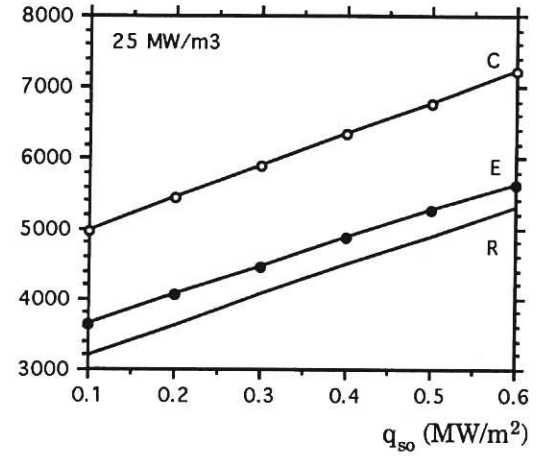

Fig. 6: The hvariation with q_{so} for the circular, rectangular and elliptical channels.

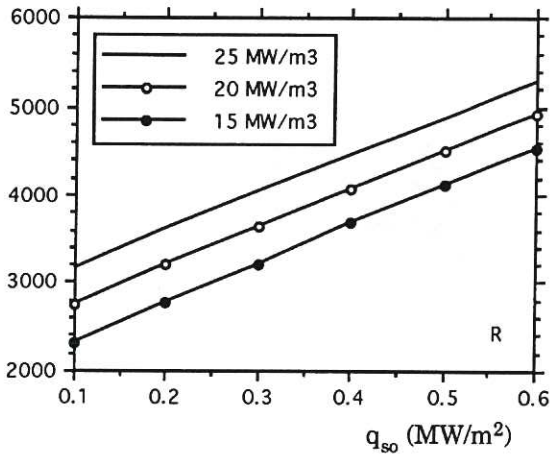

Fig. 7: The h variation with q_{so} and q_n for the rectangular channel.

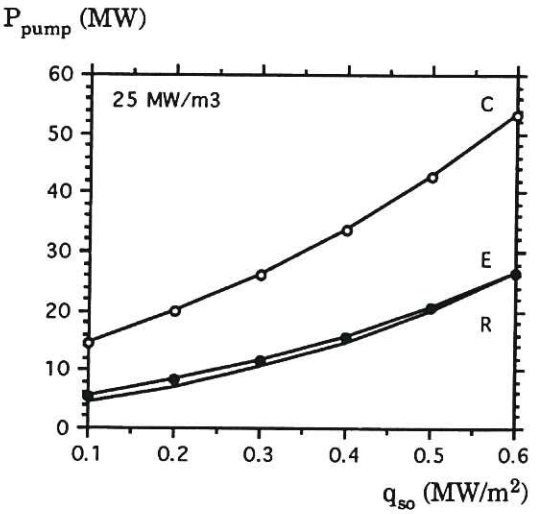

Fig. 8: The P_{pump} variation with q_{so} for the circular, rectangular and elliptical channels.

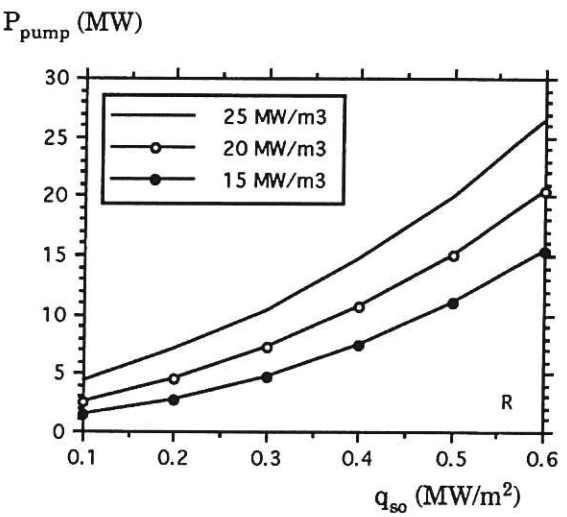

Fig. 9: The P_{pump} variation with q_{so} and q_n for the rectangular channel.

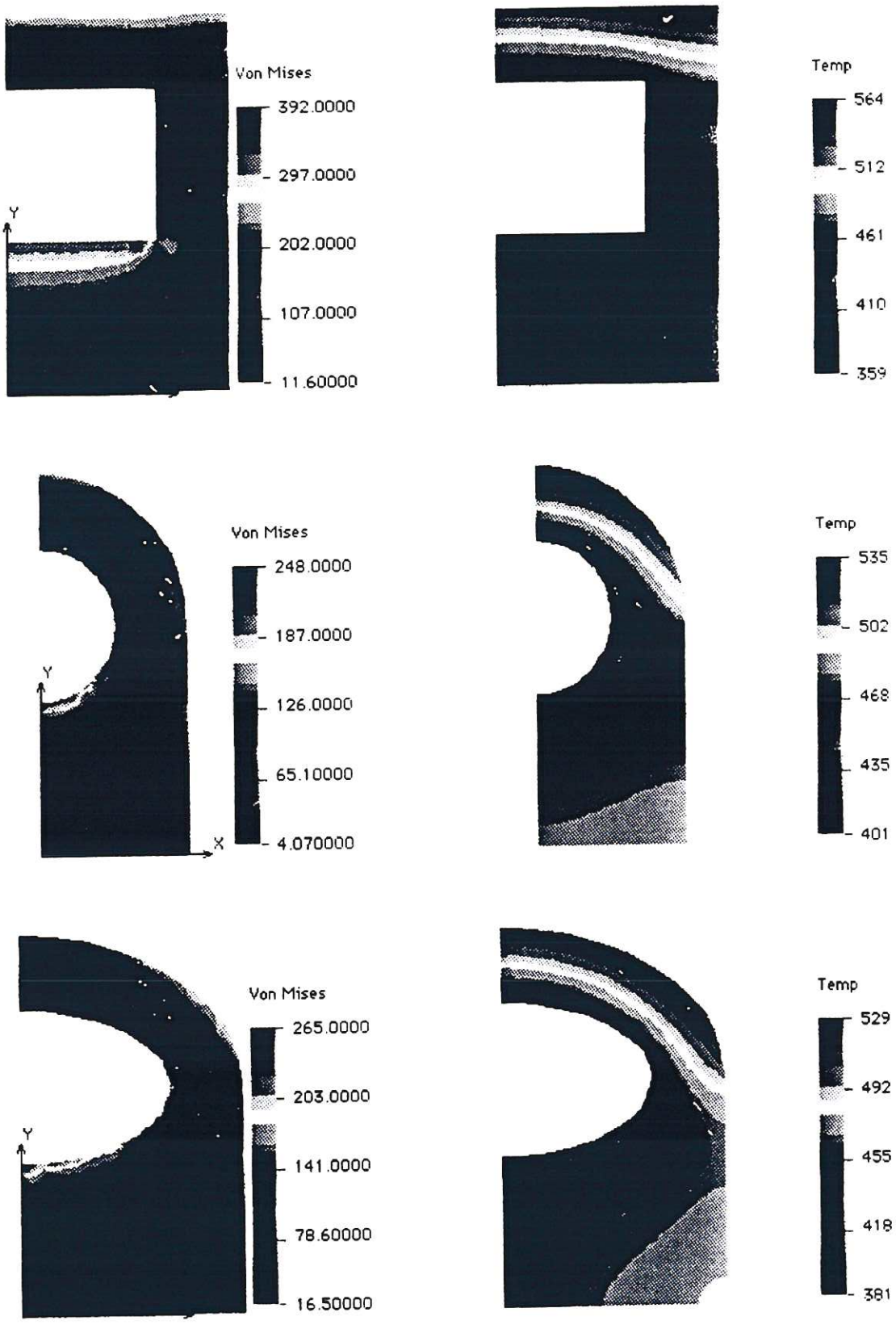

q_n=25 MW/m^3 q_{so}=0.5 MW/m^2 ΔT_c=80 K Material: MANET

Figure 10: The Von Mises thermal stress (MPa) and temperature (C) distribution for the rectangular, circular and elliptical cross section channels.

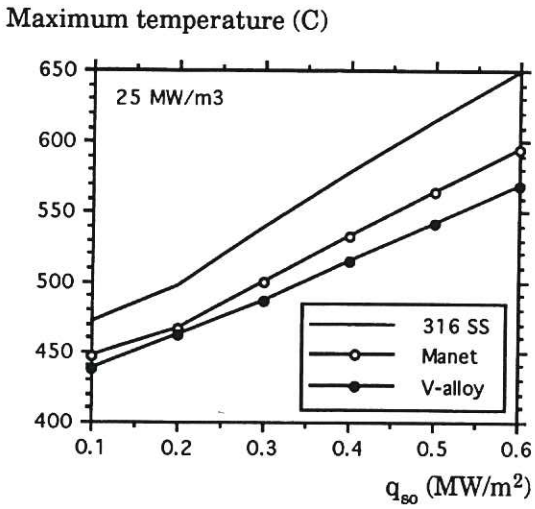

Fig. 11: Maximum temperature variation with q_{so} and material type (rectangular).

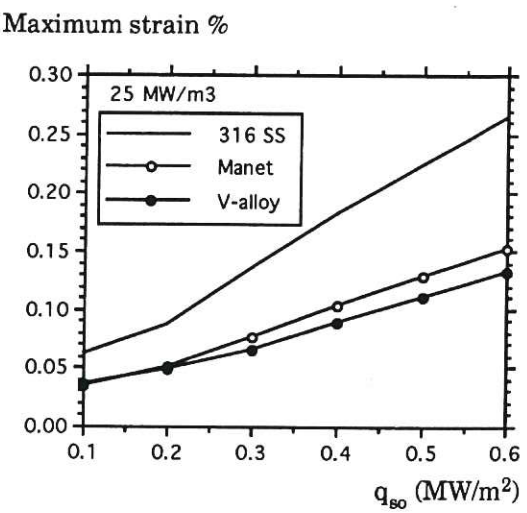

Fig. 12: Maximum strain variation with q_{so} and material type (rectangular).

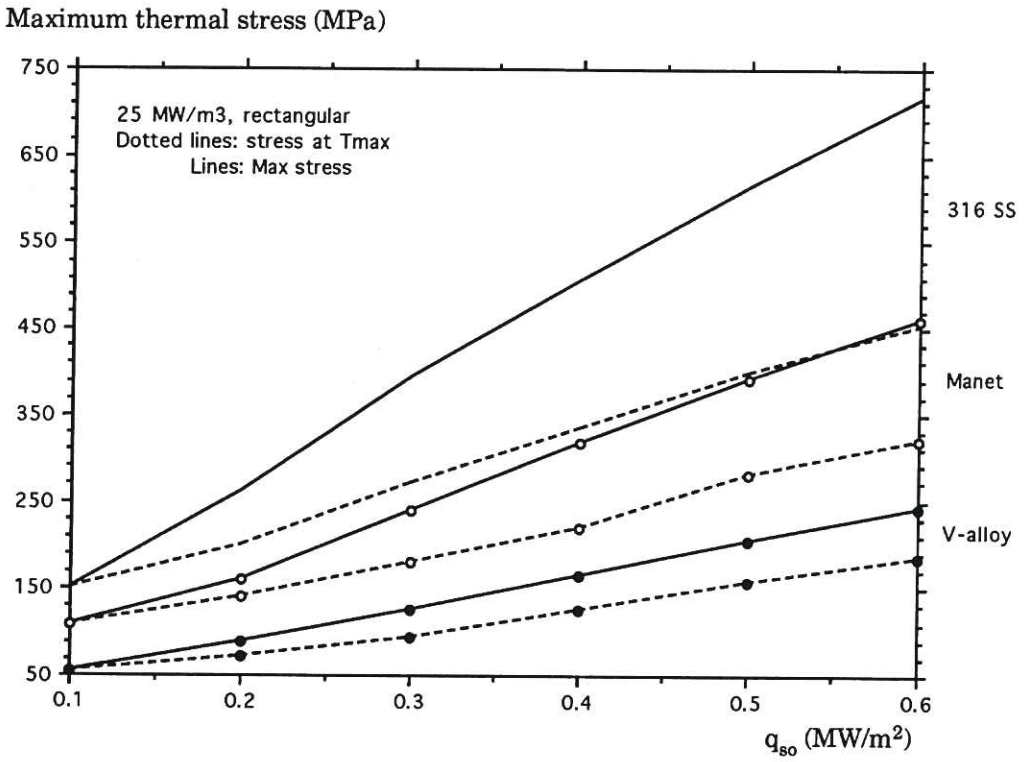

Figure 13: The Von Mises maximum and at maximum temperature thermal stress variation with q_{so} for three types of materials (rectangular channel).

REFERENCES

[1] Cooke, P.I.H.,Reynolds, P. (Eds.), "A DEMO TOKAMAK REACTOR", Rep. CLM–R254, UKAEA, Culham Laboratory, Abingdon, Oxfordshire, (1985).

[2] Commissariat a l' Energie Atomique (CEA), "DEMO-RELEVANT HELIUM COOLED SOLID BREEDER BLANKETS", Rep. DEMT 90/153, SERMA/1175, Saclay (1990).

[3] Dalle Donnne, M. (Ed.), "DEMO-relevant Test Blankets for NET/ITER", Part 2, Vol. 2, Rep. KfK 4929, Karlsruhe (1991).

[4] Casini, G. et al., "A water cooled, lithium lead breeding blanket for a DEMO fusion reactor", Fusion Engrg. Des., **14** (1991) 353-372.

[5] Mori, S., Kikuchi, M.,Seki, M., Seki, Y., "Blanket and divertor design for the Steady State Tokamak Reactor (SSTR)", Fusion Engng. Des., **18** (1991) 249-258.

[6] Institute of Plasma and Fusion Research UCLA, "THE ARIES TOKAMAK REACTOR STUDY", Rep. UCLA-PPG-1247, Los Angeles (1989).

[7] Vieider, G., Harrison, M., Moons, F., "NET Plasma Facing Components", Fusion Technology (1988), Vol. 1, 125-137.

[8] Hubert, P., "Replaceable First Walls and Thermal Re-radiation in the NET Plasma Chamber", Fusion Technology (1992), Vol. 1, 287-291.

[9] Salpietro, E. et al., "AN ALTERNATIVE FIRST WALL CONCEPT FOR NET", Fusion Technology (1992), Vol. 1, 363-366.

[10] INTERNATIONAL ATOMIC ENERGY AGENCY, ITER TOKAMAK DEVICE, ITER Documentation Series, No. 25, Vienna (1991).

[11] Sviatoslavsky, I.N., "MECHANICAL DESIGN AND FABRICATION OF THE U.S. SOLID BREEDER BLANKET FOR ITER", Fusion Technology, **19** 3,Part 2B (1991) 1552-1557.

[12] Akiyama, M. (Ed.), Design Technology of Fusion Reactors, World Scientific, Singapore (1991).

[13] ENEA, Fusion Department, Annual Report, Rome (1991).

[14] KfK, Nuclear Fusion Project, Annual Report, Karlsruhe (1991).

[15] Liew, S. L., Ku, L. P., "Three-Dimensional Monte Carlo Calculations of Nuclear Heating in CIT and Comparisons with Results from Simpler Models", Fusion Technology **19**, (1991) 1853–1858.

[16] Gallina, M., Petrizzi, L., Rado, V., "3–D MONTECARLO ANALYSIS OF THE NET SHIELDING SYSTEM", Fusion Technology (1988), Vol. 2, 1244–1248.

[17] AEA Fusion, "Pulsed fusion Reactor Study", Rep. AEA FUS 205, Culham, Abingdon, (1992).

[18] Incropera, F. P., DeWitt, D. P., Fundamentals of heat and mass transfer, John Wiley & Sons (1985) 372, 393–394.

[19] Rohsenow, W. M., Hartnett, J. P., HANDBOOK OF HEAT TRANSFER, McGraw Hill, New York (1973) 7.3–7.4, 7.27–7.33.

[20] ASME, "Boiler and Pressure Vessels Code II", American Society of Mechanical Engineers, New York (1986).

[21] BS 5500, "Unfired Fusion Welded Pressure Vessels", British Standards Institute, London (1976).

[22] ASME, "Boiler and Pressure Vessels Code, Code Case N-47", American Society of Mechanical Engineers, New York (1977).

[23] Roark, R. J., Young, W. C., Formulas for Stress and Strain, McGraw Hill, New York (1975), p. 82.

[24] Timoshenko, S. P., Goodier, J. N., Theory of Elasticity, McGraw Hill International Edition, Singapore (1970), p. 433.

[25] Munz, D., Diegele, E., "Lifetime limitation of first wall and blanket structures", Fusion Engng. Des., **16** (1991) 45-57.

[26] Stacey, W. M., FUSION, John Wiley & Sons, New York (1984) 158-170.

[27] Bressers, J. (Ed.), CREEP AND FATIGUE IN HIGH TEMPERATURE ALLOYS, Applied Science Publishers (1981).

[28] Imperial College of Science and Technology, "Stress analysis for design" course notes, Mechanical Engineering Department (1979–1980).

[29] van der Laan, J. G., et. al., "Prediction for disruption erosion of ITER plasma facing components; a comparison of experimental and numerical results", Fusion Engng. Des., **18** (1991) 135–144.

[30] Klippel, H. T., "Thermal behaviour of bare and coated first walls under severe plasma–disruption conditions", Fusion Engng. Des., **9** (1989) 49–53.

[31] Structural Research and Analysis Corp., COSMOS/M 1.65, Santa Monica, California (1992).